Wintertime decoupling of urban valley and rural ridge hydrological processes revealed through stable water isotopes

Richard P. Fiorella[1], Ryan Bares[2], John C. Lin[2,3], and Gabriel J. Bowen[1,3]

1: Department of Geology and Geophysics, University of Utah, 115 S 1460 E, Salt Lake City, UT 84112

2: Department of Atmospheric Sciences, University of Utah, Salt Lake City, UT

3: Global Change and Sustainability Center, University of Utah, Salt Lake City, UT

Corresponding author: Rich Fiorella, rich.fiorella@utah.edu

Abstract

Water from fossil fuel combustion can represent >10% of urban specific humidity, but this fraction is difficult to constrain from meteorological measurements alone. Stable water vapor isotopes can be used to estimate the fraction of combustion-derived vapor (CDV) and characterize the contrast between anthropogenically-altered and natural systems due to CDV's distinctive isotope composition. However, accurate estimates of the CDV fraction of urban humidity requires information on vapor isotope ratios in the absence of anthropogenic emissions. We present data from an urban site in Salt Lake City, UT and from a high-elevation site in the adjacent Wasatch Mountains. Urban vapor d-excess values (d-excess = $\delta^2H–8\delta^{18}O$) closely track CO_2 concentrations on diurnal to weekly timescales, but high-elevation vapor values do not. Instead, the high-elevation site captures large-scale atmospheric variability, with d-excess changes largely following changes in $\delta^{18}O$ and humidity. Isotope ratios at the two sites remain distinct throughout most of the winter, indicating that these sites are regularly decoupled from each other and that high-elevation winter measurements may rarely be representative of valley conditions in the absence of urban emissions. Furthermore, high-elevation d-excess may be higher than emissions-free values at the same elevation as the urban area, as vapor d-excess changes non-linearly during condensation at low specific humidity, and would result in an overestimate of urban humidity amounts. Therefore, the high-elevation site may not help place additional constraints on the amount of CDV in urban systems, yet the paired sites show changes in vapor isotope ratios, particularly in d-excess, that capture differences in urban and natural impacts on water vapor cycling.

1. Introduction

Boundary layer specific humidity over cities is often ~10% higher than the surrounding rural areas during winter (Ackerman, 1987; Bergeron and Strachan, 2012; Hage, 1975; Hall et al., 2016; Kuttler et al., 2007; Liu et al., 2009; Moriwaki et al., 2008; Salmon et al., 2017). Several possible mechanisms have been proposed to explain this urban humidity excess, including changes in the diurnal energy budget (e.g., Bengtsson and Westerström, 1992), increased evaporation due to the urban heat island effect (e.g., Bergeron and Strachan, 2012) or by direct water emissions from evaporative cooling towers (Moriwaki et al., 2008), and fossil fuel combustion, which releases water vapor as a byproduct (Ackerman, 1987; Fiorella et al., 2018a; Gorski et al., 2015; Hage, 1975). However, the source(s) of the increased humidity are difficult to determine solely from meteorological measurements.

Stable water vapor isotopes can potentially apportion urban humidity between combustion-derived vapor (CDV) and "natural" components. CDV inherits its isotopic composition from the reaction of atmospheric oxygen, which has a near-constant $\delta^{18}O$ value of +23.9‰ (Barkan and Luz, 2005), with hydrogen in fuels, which is depleted in ^{2}H due to photosynthetic preference for ^{1}H (e.g., Estep and Hoering, 1980). The resulting vapor isotope ratios are unusual in the "natural" hydrological cycle, and are most distinctly expressed in the d-excess ($d = \delta^{2}H - 8\delta^{18}O$) (Dansgaard, 1964) value (Fiorella et al., 2018a; Gorski et al., 2015). Natural d-excess values range from ~ +300‰ in vapor in the upper tropical troposphere (Bony et al., 2008; Webster and Heymsfield, 2003) to ~ –60‰ in highly evaporated surface waters (e.g., Fiorella et al., 2015), though d-excess is typically ~10‰ in precipitation (Dansgaard, 1964). In contrast, theoretical estimates for CDV d-excess values are substantially more negative. Informative but weak constraints can be placed on the d-excess of CDV from theory (Gorski et al., 2015) or Keeling-style inversions of observed d-excess under stable atmospheric conditions

(Fiorella et al., 2018a). For example, combustion of fuels for the Salt Lake City, Utah area yield estimates of CDV d-excess from –470 to –180‰ (Gorski et al., 2015). These estimates are supported by a limited number of direct measurements of CDV (Gorski et al., 2015), and a Keeling-style (1961, 1958) estimation of -179±17‰ for CDV d-excess in the Salt Lake Valley (Fiorella et al., 2018a).

These constraints on CDV d-excess have been used in two prior studies of water vapor isotope ratios in Salt Lake City, Utah, United States. Located in a topographic basin, the Salt Lake Valley experiences multiday periods where CO_2, CDV, and air pollutants are often strongly elevated due to high atmospheric stability arising from the emplacement of "persistent cold air pools" (PCAPs) (Baasandorj et al., 2017; Fiorella et al., 2018a; Whiteman et al., 2014). The urban humidity fraction originating from CDV can be determined using a mixing model between background water vapor and CDV. Writing two mass balance equations for bulk humidity and its d-excess value yields:

$$q_{obs} = q_{nat} + q_{CDV} \quad (1)$$

$$q_{obs} d_{obs} = q_{nat} d_{nat} + q_{CDV} d_{CDV} \quad (2)$$

where subscripts obs, nat, and CDV refer to the observed, natural, and CDV constituents respectively, d is the d-excess value, and q is the specific humidity. The fraction of urban humidity arising from combustion can then be expressed by solving the system of equations #1-2 for q_{CDV}/q_{obs}:

$$\frac{q_{CDV}}{q_{obs}} = \frac{d_{obs} - d_{nat}}{d_{CDV} - d_{nat}} \quad (3)$$

The mixed or observed parcel can be directly measured in the urban environment; however, the d-excess of the natural and CDV components must be measured independently or given an assumed value. This situation is analogous to that encountered in urban CO_2 studies, which also

93 require estimation of a background CO_2 value to estimate emissions inputs (Bares et al., 2018;
94 Duren and Miller, 2012; Lauvaux et al., 2016; Mitchell et al., 2018; Super et al., 2017; Turnbull
95 et al., 2011; Verhulst et al., 2017). These prior vapor isotope studies in the Salt Lake Valley
96 indicate that up to ~16% of urban humidity during PCAP events may arise from combustion
97 (Fiorella et al., 2018a; Gorski et al., 2015).

98 One major source of uncertainty in these estimates, however, is that the d-excess of
99 natural water vapor varies through time (Aemisegger et al., 2014; Fiorella et al., 2018b), and
100 these variations are not known from measurements within the urban area. Gorski et al. (2015)
101 applied a smoothing spline to d-excess outside of PCAP events, when the effect of emissions is
102 expected to be low, to estimate natural d-excess variations during PCAP events. In contrast,
103 Fiorella et al. (2018a) tested two different constraints on natural d-excess: a) using the measured
104 d-excess value prior to emplacement of the PCAP, and b) using the measured d-excess from
105 when pCO_2 was last below 415 ppm, taken to reflect well-mixed conditions without substantial
106 enhancement of pollutants. These assumptions and have not been empirically validated with
107 simultaneous measurements of d-excess in an emissions-free area and require that natural d-
108 excess is either invariant or smoothly varying through the PCAP event.

109 Here, we hypothesize that water vapor isotope measurements from a nearby high-
110 elevation site, which remains above the stable boundary layer during PCAP events, can provide
111 an improved estimate of background variability in atmospheric d-excess. We test this hypothesis
112 by comparing water isotope ratios during DJF 2016-2017 from two closely located sites in the
113 Salt Lake City area: one within the urban basin (UOU, Fig. 1) and the other at a high elevation
114 site in the adjacent Wasatch Mountains (HDP, Fig. 1). We find a strong relationship between
115 CO_2 and vapor d-excess at UOU, but not at HDP. Instead, HDP d-excess responds to

meteorological variability and not anthropogenic factors. However, in contrast to our hypothesis, HDP d-excess values fail to provide a stronger constraint on natural d-excess values in the Salt Lake Valley, as the high-elevation and valley systems are decoupled throughout most of the winter. Condensation at low humidity values causes vapor d-excess to increase non-linearly, causing d-excess values at HDP to likely exceed d_{nat} in the Salt Lake Valley; using these values in equation 3 for d_{nat} would therefore overestimate q_{CDV}/q_{obs}. Finally, we discuss the implications of these results for future studies of CDV in urban systems.

2. Methods

2.1. Water Vapor Isotope Measurements

We measured the isotopic composition of atmospheric water vapor from DJF 2016-2017 at the top of the William Browning Building (~33 m above ground level) on the University of Utah campus (UOU, 40.7662°N, 111.8478°W, 1440 m above sea level) and at the summit of Hidden Peak (HDP, 40.5608°N, 111.6450°W, 3350 m above sea level) at the Snowbird Resort in Alta, Utah, United States (Fig. 1). The UOU site has operated with water vapor isotopes since December 2013, while HDP was installed on 8 December 2016. Water vapor isotopic compositions were measured by Picarro L2130-i analyzers. Vapor was sampled passively through ¼" PTFE tubing at UOU and ¼" HDPE tubing at HDP, with a swinging piston pump pulling air through the tubing at ~3 L/min. The HDP tubing was lightly heated with a trace cable, as the inlet otherwise would become covered in rime ice; no such limitation was observed at UOU. Condensation in the sampling line at the UOU site, had it occurred, would have increased vapor d-excess. Therefore, our choice to leave the UOU sampling inlet unheated cannot explain our measurements of negative d-excess values when ambient pCO_2 is high.

Calibration of raw Picarro isotope measurements to the VSMOW-VSLAP scale occurred in two steps. First, measured isotope ratios of standard waters exhibit a bias proportional to cavity humidity in laser-based water isotope analyzers (Bailey et al., 2015a; Gupta et al., 2009; Schmidt et al., 2010; Steen-Larsen et al., 2014). To remove this instrumental bias, we measured a laboratory standard across a wide range of humidities to generate correction equations for instrument-specific bias due to cavity humidity using weighted least-squares regression. Full details of this regression are given in the Supplemental Text. Second, measurements are calibrated to the VSMOW-VSLAP scale via linear regression between measured and known isotope values of standards for periods bracketing the ambient measurement periods. Two isotopic standards were measured every 12 hours (Table 1), and were introduced to the analyzer cavity by the Picarro Standard Delivery Module (Picarro Part A0101) via the Picarro High Precision Vaporizer (Picarro Part A0211), which was maintained at 140°C to flash vaporize introduced water standards. Standard waters bracketed the range of isotope ratios observed at the HDP site, but observed isotope ratios at the UOU site were often more negative than the most negative standard. As a result, isotope ratios at the UOU site were extrapolated from the range of isotope ratios in the two standards, which will introduce an additional source of error. As the Picarro cavity ring-down instrument produces highly linear measurements of isotope ratios in water vapor at the same concentration (e.g., Aemisegger et al., 2012; Schmidt et al., 2010), we expect this source of error to be small.

The background carrier gas during calibration measurements was laboratory air drawn through a desiccation column filled with anhydrous calcium sulfate (Drierite, W.A. Hammond Co., Item Number 26840). Variations in the composition of background gases can cause apparent changes in measured oxygen and hydrogen isotope ratios without any changes in the water vapor

isotope ratios (Gralher et al., 2016; Hendry et al., 2011; Johnson and Rella, 2017). Though concentrations of some of the background gases do vary throughout these observations (e.g., CO_2 and CH_4), these changes are small relative to (i.e., ≥2 orders of magnitude smaller than) changes that have been documented to produce permil-level shifts in measured water isotope ratios in these studies. Therefore, we do not consider potential biases from changes in background gas concentrations further. Full details of our sensitivity analysis to these gases is provided in the Supplemental Text.

We estimated total instrument uncertainty as a function of cavity humidity by combining estimated errors from the humidity-bias correction equation and instrumental noise, estimated as the standard deviation of standard measurements at each humidity level; full details are given in the Supplemental Text. As the humidity-bias correction equation error already includes some measure of instrumental noise from the weighted least-squares fitting procedure, these error estimates are conservative and may be larger than the true error. At 3000 ppmv, a humidity commonly observed at both sites during these measurements, 1σ uncertainty for $\delta^{18}O$, $\delta^{2}H$, and d-excess were 0.4‰, 2.0‰, and 3.9‰ at HDP and 0.6‰, 2.1‰, and 5.3‰ for UOU respectively.

2.2. CO_2 and Meteorological Measurements

CO_2 and H_2O mole fractions were measured at 10-second intervals for both sites using a Los Gatos Research UltraPortable Greenhouse Gas Spectrometer (Model 907-0011). Water vapor dilution and spectrum broadening effects on CO_2 measurements were corrected with on-board software produced by Los Gatos Research, and independently verified by laboratory testing. Three whole-air, high-pressure calibration gases with known CO_2 concentrations

185 spanning the range of atmospheric observations (directly linked to WMO X2007 mole fraction
186 scale; Zhao and Tans, 2006) were introduced in series to the analyzer every three hours, at
187 approximately 400, 475 and 525 ppm respectively.

188 UOU meteorological measurements (Horel et al., 2002) are co-located with CO_2 and
189 water vapor isotope observations. HDP weather measurements are from the Mt. Baldy summit,
190 0.25 km east of and ~200 m above HDP. All specific and relative humidity, temperature, and
191 wind speed data presented in our analysis are from these meteorological observations. We
192 calculate potential temperature using measured atmospheric pressure at UOU and assume a
193 constant pressure of 650 hPa for HDP, estimated from elevation using the 1976 U.S. Standard
194 Atmosphere.

195 We assessed atmospheric stability using two metrics derived from twice daily (00 and 12
196 UTC) radiosonde data from the Salt Lake City International Airport (KSLC, Fig. 1): the valley
197 heat deficit and the estimated mixing height. Sounding profiles were interpolated to 10 m
198 intervals from the surface (1290 m) to 5000 m. Valley heat deficit, which reflects the heat
199 required to bring the atmospheric column between the surface and 2200 m to the dry adiabatic
200 lapse rate (Baasandorj et al., 2017; Whiteman et al., 2014), is calculated as:

201 $$VHD = c_p \sum_{1290\,m}^{2200\,m} \rho(z)[\theta_{2200\,m} - \theta(z)]\Delta z \quad [\mathrm{J\ m^2}] \qquad (4)$$

202 where c_p is the dry air heat capacity (J kg^{-1} K^{-1}), ρ(z) is the air density at height z (kg m^{-3}), θ is
203 the potential temperature, and Δz is the layer thickness (10 m). Following previous studies in the
204 Salt Lake Valley, we define a PCAP event as three consecutive soundings where the valley heat
205 deficit exceeded 4.04 MJ m^{-2} (Baasandorj et al., 2017; Bares et al., 2018; Whiteman et al., 2014).
206 High atmospheric stability leading to PCAP events typically arises from surface cooling

associated with snow cover and cold air drainage or warming aloft from emplacement of an upper-level ridge (Bailey et al., 2011; Whiteman et al., 2014; Wolyn and McKee, 1989). PCAPs often feature a temperature inversion near the surface, with warmer air sitting atop colder air, though substantial valley heat deficits can result from an isothermal atmospheric column as well (Whiteman et al., 2014).

A bulk Richardson number is used to estimate the mixing height (e.g., Seidel et al., 2012):

$$Ri(z) = \frac{\left(\frac{g}{\theta_{vs}}\right)(\theta_v(z) - \theta_{vs})(z - z_s)}{(u(z) - u_s)^2 + (v(z) - v_s)^2 + (bu_*^2)} \quad (5)$$

where g is the acceleration due to gravity (m s^{-2}), θ_v is the virtual potential temperature (K), z is the altitude (m ASL), u and v are the zonal and meridional wind components (m s^{-1}), and bu^2_* is a surface friction term. We assume negligible surface friction ($bu_*^2 = 0$), which is appropriate in stable atmospheric layers such as PCAPs (Vogelezang and Holtslag, 1996). The subscript 's' indicates surface values. The mixing height is assigned as the lowest altitude where Ri(z) > 0.25. Mixing heights are reported as meters above sea level instead of meters above ground level to facilitate comparison with the altitudes of UOU (1440 m ASL) and HDP (3350 m ASL).

2.3. Data analysis

Data were processed and plotted using the R language and tidyverse packages (R Core Team, 2019; Wickham and Grolemund, 2016). Water vapor isotope, CO_2, and meteorology data streams were averaged to a common hourly interval. Wavelet power spectra were calculated for the d-excess time series using the WaveletComp package (Rösch and Schmidbauer, 2016). Wavelet transforms decompose a time series into a 2D-matrix of time and frequency, and permit

229 analysis of the dominant frequencies in a time series, and these dominant frequencies vary
230 through time (Torrence and Compo, 1998). We used the Morlet wavelet, which includes both
231 positive and negative oscillations of a frequency in the calculation of wavelet power. Other
232 wavelet basis functions, such as the derivative of a Gaussian function, capture both positive and
233 negative extrema as separate peaks in the wavelet power spectrum. As a result, regions of high
234 spectral power at a certain frequency plot as a single broad peak in this analysis instead of
235 several high-power oscillations. Coherence between UOU d-excess and CO_2 concentrations were
236 evaluated using wavelet cross-spectra, with arrows to indicate the phase relationship.

237 Relationships between vapor d-excess, $\delta^{18}O$, q, relative humidity, CO_2 concentration, and
238 500 hPa vertical velocity were analyzed with a principal component analysis. In brief, principal
239 component analysis decomposes a series of correlated variables along a smaller set of
240 orthogonal, uncorrelated variables called principal components (Venables and Ripley, 2002). We
241 use principal components analysis here to understand how meteorological variables covary with
242 water vapor isotope ratios and CO_2, and the use of multiple principal components provides a
243 sense of different modes in which this suite of variables can covary. Vertical velocity was
244 extracted from the nearest grid cell of the 6-hourly ERA-Interim dataset (Dee et al., 2011), and
245 interpolated to an hourly time step to match the frequency of the meteorological and isotopic
246 data. All principal components with an eigenvalue greater than one were retained (Kaiser, 1958),
247 giving three principal components explaining >80% of the total variance at each site.

248 Simple stable water vapor isotope models were constructed and correspond to Rayleigh
249 distillation (condensation and removal of water under saturated conditions) or the mixing of
250 moist and dry air masses (following Bailey et al., 2015b; Noone, 2012). Initial conditions for the
251 moist air mass prior to condensation or mixing corresponded to vapor at saturation with a $\delta^{18}O$

252 value in isotopic equilibrium with ocean water ($\delta^{18}O$ = 0.0‰) at 25°C, using fractionation
253 factors from Horita and Wesolowski (1994). The initial vapor $\delta^{2}H$ value was chosen to give the
254 initial vapor d-excess a value of 10‰ to mimic the mean value from the global meteoric water
255 line (Dansgaard, 1964). Finally, a second mixing model was produced illustrating the addition of
256 0–500 ppmv of CDV, where d_{CDV} was assumed to be –179 ± 17‰ (Fiorella et al., 2018a). This
257 estimate of d_{CDV} is derived from a prior Keeling-style inversion of vapor isotope measurements
258 in the Salt Lake Valley (Fiorella et al., 2018a), and is consistent with the upper-limit of d_{CDV}
259 values proposed by Gorski et al. (2015). No explicit assumption about the associated $\delta^{18}O$ and
260 $\delta^{2}H$ values are made, though the $\delta^{18}O$ is expected to be between ca. -5 and 23.9‰ depending on
261 the extent of equilibration between CO_2 and H_2O in the combustion exhaust (Gorski et al., 2015),
262 and the $\delta^{2}H$ is expected to mirror the hydrogen isotope ratio of the fuel. For Salt Lake City, we
263 expect fuel $\delta^{2}H$ values of ca. -150 to -200‰ $\delta^{2}H$ (Gorski et al., 2015; Whiticar, 1999). As these
264 oxygen and hydrogen isotope ratios are not unusual, we do not expect the non-linear nature of
265 the delta scale at extreme delta values (e.g., Dütsch et al., 2017) to influence our results.
266
267 **3. Results**
268 Eight PCAP events occurred during DJF 2016-2017 (Fig. 2a). The second and third
269 events were separated by a single sounding with a valley heat deficit < 4.04 MJ m^{-2} and are
270 labeled as PCAP 2a and 2b. PCAPs 1, 2a, 3, 4, and 5 lasted for three consecutive soundings,
271 while PCAPs 2b, 6, and 7 extended for eight, nine, and five soundings, respectively. HDP $\delta^{18}O$
272 and $\delta^{2}H$ values were nearly always lower than those at UOU and exhibited higher variability
273 (Fig. 2b). Hourly UOU $\delta^{18}O$ ($\delta^{2}H$) compositions averaged –25.8±3.3‰ (–208.6±28.7‰),
274 whereas hourly HDP compositions averaged –30.6±5.0‰ (–230.6±35.7‰). D-excess values

were higher at HDP than UOU, averaging 13.9±5.9‰ and –2.0±5.8‰ respectively (Fig. 2c). D-excess values at HDP were consistently ~15‰ greater than at UOU through December and January before converging in early February (Fig 2c), with the most pronounced differences occurring when valley heat deficit was low and mixing heights were elevated (Fig. 2a). CO_2 concentrations averaged 439±30 ppm at UOU and 410±3 ppm at HDP. UOU CO_2 concentrations were generally higher than those at HDP; this effect was most prominent when valley heat deficit was high and/or mixing height was low, such as during PCAP events (Fig. 2d). Prior studies in the Salt Lake Valley have demonstrated strong covariance between elevated urban CO_2 and other indicators of combustion such as carbon monoxide and nitrogen oxides (Baasandorj et al., 2017; Bares et al., 2018). Potential temperature exhibited similar trends at both sites except during and immediately surrounding PCAP events (Fig. 2e) when HDP potential temperature often increased, perhaps due to large-scale subsidence. HDP was drier than UOU, with specific humidity averaging 1.9±0.9 g kg^{-1} at HDP and 3.0±1.1 g kg^{-1} at UOU (Fig. 2f). The lower specific humidity at HDP compared to UOU is likely a primary factor responsible for the lower and more variable $\delta^{18}O$ values, as small changes in humidity through mixing or condensation processes can induce large isotope ratio responses when humidity is low. Mean relative humidity was similar between the two sites, 72±25% for HDP and 68±18% for UOU (Fig. 2g), except during PCAP events, when relative humidity at HDP often decreased concurrent with an increase in potential temperature (Fig. 2e) and/or a decrease in specific humidity (Fig. 2f). Wind speeds were generally higher at HDP than at UOU (Fig. 2h), and reached a maximum value of 13 m/s at HDP and 7 m/s at UOU. Finally, 500 hPa vertical velocity, estimated from ERA-Interim (Dee et al., 2011), varied between 0.3 and -0.8 Pa/s (Fig. 2i). PCAP events tended to follow periods of atmospheric subsidence (500 hPa vertical velocity > 0 Pa/s), but not every period of subsidence

298 of triggered a PCAP event. This result highlights the complex nature of PCAP initiation, which
299 is known to be influenced by snow cover, solar radiation, and local-scale interactions between
300 topography and air masses (Whiteman et al., 2014).
301
302 *3.1. Do HDP d-excess measurements provide an improved estimate of d_{nat}?*
303 We hypothesized that d-excess measurements out of the valley and above the inversion
304 characteristic of most PCAP events might provide improved constraints on d_{nat}; here we compare
305 calculations of the CDV humidity fraction from estimates of d_{nat} from both UOU and HDP.
306 Estimated CDV fractions of urban humidity ranged from -1.9±6.9% to 9.0±5.6% when d_{nat} was
307 estimated from pre-PCAP d-excess at UOU, while d_{nat} was estimated from pre-PCAP d-excess at
308 HDP yielded estimates ranging from 8.9±3.5% to 22.7±5.4% (Table 2). Negative CDV fractions
309 estimated using d_{nat} estimates from UOU clearly highlight the difficulty of using water vapor
310 isotope measurements within the urban footprint to calculate the fraction of vapor from
311 combustion. In contrast, CDV fractions calculated from HDP d_{nat} estimates were uniformly
312 positive, but large. We produced estimates of CDV amounts in ppm from these CDV fractions,
313 and compared them to the concurrent CO_2 concentration (Fig. 3). Increases in CO_2 and CDV
314 above background values should be proportional, and the ratio of H_2O to CO_2 in combustion
315 exhaust depends on the stoichiometry of the fuels used. Fiorella et al. (2018a) estimated this ratio
316 to be 1.5 for Salt Lake Valley based on an accounting of emissions sources from HESTIA,
317 though values from 1 (approximating coal emissions) to 2 (corresponding to methane
318 combustion) are reasonable. CDV predictions made from HDP d-excess uniformly require this
319 ratio to be greater than 2 (Fig. 3), indicating that HDP d-excess is unlikely to provide improved
320 constraints on the estimate of d_{nat}. In contrast, CDV amount estimates made from pre-event UOU

d-excess do suggest a molar ratio of CDV:CO_2 between 1 and 2 in emissions. This is expected, however, since our d_{CDV} estimate of -179±17‰ assumes a molar ratio of 1.5 and is determined from an inversion of d-excess measurements at UOU (Fiorella et al., 2018a). Though the HDP measurements do not provide an independent validation of d_{nat}, both sites do show clear but distinct variability in d-excess. The following section examines the response of d-excess to changes in CO_2 and meteorological variables at the two sites.

3.2. Factors influencing d-excess at UOU and HDP

UOU and HDP d-excess values vary at different frequencies throughout the season, and their variation arises from distinct causes. Below, we analyze the frequency response using wavelets and explore relationship between d-excess and CO_2 and meteorological variables using principal component analysis. Wavelet analysis of the d-excess spectra indicated distinct characteristic periodicities for each site. UOU d-excess exhibited significant spectral power at multi-day to weekly timescales, and episodically at diurnal timescales (Fig. 4a). Strong diurnal spectral power at UOU was closely associated with periods where CO_2 was elevated for multiple days, and always during PCAP events (Fig. 4a). Significant diurnal spectral power was also observed at HDP, but was often displaced from PCAP events (e.g., PCAP 2b and 7; Fig. 4b) and was also observed outside of PCAP events (e.g., between PCAP 1 and 2a; Fig. 4b). At both sites, significant spectral power was observed on timescales of multiple days. The high spectral power at periods of multiple days to weeks follows expectations for a red noise process, and likely results from large-scale transport and moisture source influences on d-excess (Aemisegger et al., 2014).

A strong inverse correlation between CO_2 concentration and d-excess was observed at UOU across the time series (r = –0.65). Cross-wavelet spectral power between UOU d-excess and CO_2 suggests a robust inverse relationship on diurnal timescales when CO_2 was elevated and on multiday-to-weekly timescales across the record (Fig. 4c). Correlation of low d-excess values and high CO_2 concentrations strongly suggests that combustion-derived vapor, which has a low d-excess, was present at UOU when CO_2 was elevated (Fiorella et al., 2018a; Gorski et al., 2015). Variability in CO_2 was an order of magnitude lower at HDP than at UOU (Fig. 2d), whereas variability in d-excess was of comparable magnitude (Fig. 2c). No consistent phase relationship between CO_2 and d-excess was found at HDP. Therefore, changes in d-excess are strongly coupled to changes in CO_2 at UOU, but changes at HDP are presumably related to variations in regional fetch history or natural hydrological processes.

The first three principal components (PCs) of the data from each site illustrate the factors strongly influencing d-excess (Fig. 5). The inverse relationship between UOU CO_2 and d-excess manifests as strong but opposing loadings onto PCs 1, 2, and 3 (Fig. 5ab). Correlations between other meteorological variables and d-excess at UOU were weak and inconsistent across all three PCs (Fig. 5ab). UOU specific humidity partitioned into two modes, one dominantly controlled by vertical velocity (Fig. 5a) and the other controlled by combustion and CO_2 (Fig. 5b). Data during PCAP events varied along the CO_2 axis for all three PCs and diverged from the other portions of the dataset along PCs 1 and 2 (Fig. 5ab). Positive correlations between UOU $\delta^{18}O$ and specific humidity were observed on all three PCs, and this relationship was independent of the other variables analyzed (Fig. 5abc).

In contrast, HDP $\delta^{18}O$ exhibited a strong negative correlation with d-excess, as shown by the strong opposing loadings onto PCs 1 and 2 (Fig. 5c). A strong inverse relationship between

366 the 500 hPa vertical velocity and relative humidity orthogonal to the d-excess-$\delta^{18}O$ axis was
367 observed, indicating that large-scale atmospheric motion impacted the RH at HDP (Fig. 5c).
368 However, correlations between 500 hPa vertical velocity and $\delta^{18}O$ (r = -0.11) and d-excess (r =
369 0.01) at HDP were weak. Variation along the first two PCs at HDP indicate two distinct
370 relationships between large-scale atmospheric motion, humidity, and vapor isotope ratios: (1)
371 atmospheric subsidence (uplift) increases (decreases) d-excess but decreases (increases) specific
372 humidity, relative humidity, and $\delta^{18}O$, as suggested by PC1, and (2) atmospheric subsidence
373 (uplift) increases (decreases) $\delta^{18}O$ but decreases (increases) relative humidity and d-excess, with
374 little impact on specific humidity, as suggested by PC2 (Fig. 5c). These patterns suggest that two
375 distinct methods of environmental variability promote covariation between d-excess, relative
376 humidity, $\delta^{18}O$, and 500 hPa vertical velocity. Examination of time series of PC1 and PC2
377 suggests that the first mode is closely associated with PCAP events, while the second mode is
378 more closely related to the complex boundary layer structures observed in late December, where
379 large and diurnal swings in relative humidity are observed. PCAP and non-PCAP periods
380 diverged along the vertical velocity axis, indicating that the primary response at HDP during
381 PCAP events reflected strong atmospheric subsidence (Fig. 5cd). Strong atmospheric subsidence,
382 in response to surface cooling and/or warming aloft, likely plays a role in PCAP initiation (e.g.,
383 Whiteman et al., 2014) and is likely responsible for the coupled d-excess changes between sites
384 despite distinct responses to changes in meteorological variables and CO_2 concentrations.
385 Indeed, in contrast to UOU, HDP CO_2 had little impact on PC1, had only a small loading of HDP
386 CO_2 was observed on PC2, and only had a larger loading on PC3 (Fig. 5c).
387 Isotope process models also clearly show the distinct response of urban water vapor at
388 UOU during the winter relative to the high elevation HDP measurements. UOU d-excess values

were most consistent with natural processes of condensation (modeled via Rayleigh distillation) and mixing when CO_2 was not strongly elevated (Fig. 6a). Deviation in d-excess values from these natural process models scaled with urban CO_2 concentrations. The most negative d-excess values were observed when specific humidity was low and CO_2 was high, when the added CDV would comprise the largest fraction of total humidity and induce the largest isotopic response (Fig. 6a) (Fiorella et al., 2018a). In contrast, HDP d-excess generally followed the Rayleigh / air mass mixing models, with no clear excursions along CDV-mixing lines (Fig. 6b). This trend further suggests that HDP d-excess is generally controlled by natural water cycle processes and is minimally impacted by urban emissions.

The joint distribution of d-excess and $\delta^{18}O$ represents a complimentary approach to examine variability between the UOU and HDP sites. Neglecting CDV addition and continental recycling of vapor, which likely has a limited impact on winter vapor isotope ratios (Aemisegger et al., 2014; Fiorella et al., 2018b; van der Ent et al., 2010), Rayleigh distillation and mixing between tropical and dry continental end members produce the lowest and highest $\delta^{18}O$ and d-excess values for a given specific humidity, respectively. Isotope ratios intermediate to these modeled compositions can be obtained by mixing of any number of air masses over the continent. As a result, natural condensation and mixing processes should result in isotope ratios within a region delineated by Rayleigh and tropical-dry continental mixing models. Addition of CDV should decrease d-excess, and pull isotope ratios out of these constraints. We observe that HDP isotope ratios generally fall within the "natural" joint isotope distribution, while UOU isotope ratios do not (Fig. 6cd). Furthermore, the distance from the natural joint isotope distribution region for UOU is proportional to urban CO_2 levels (Fig. 6c), providing further

support that UOU isotope ratios are pervasively influenced by CDV while HDP isotope ratios are not (Fig. 6d).

4. Discussion

Stable water vapor isotopes represent a promising tool to estimate the fraction of urban humidity arising from combustion. The robust coherence between urban CO_2 and d-excess has been consistently observed across four Salt Lake City winters (this study; Fiorella et al., 2018a; Gorski et al., 2015), and strongly suggests that CDV is detectable. We found that variability in d-excess occurs at different frequencies between the two sites, and correlates most strongly with meteorological variables at HDP while UOU d-excess correlates most strongly with CO_2 (Fig. 5). Further, we demonstrated using joint isotope distributions that patterns of d-excess and $\delta^{18}O$ in vapor are consistent with natural advection and condensation processes at HDP, but not at UOU (Fig. 6c).

Both sites exhibit high spectral power at low frequencies, but different patterns dominate high frequency variability between these sites. High spectral power in d-excess at low frequencies likely reflects variability in response to weather events, such as frontal passage associated with winter storms (e.g., Aemisegger et al., 2015; Graf et al., 2019) (Fig. 2i). Responses to storm cycles occur at synoptic frequencies, and consistently are associated with negative excursions in $\delta^{18}O$ and lower specific humidity at both sites (e.g., ahead of PCAPs 1, 2a, 3, and 6, Fig. 2b,f). In contrast, high frequency cyclicity in d-excess is likely driven by distinct processes at each site throughout the record. Diurnal-scale d-excess cyclicity is strongly associated with elevated CO_2 and PCAP events at UOU. The HDP d-excess record also exhibits periods of strong diurnal-and-higher frequency cyclicity, however, despite little change in CO_2

concentrations (Fig. 2cd). Changes in HDP d-excess arising from CDV associated with the small changes in CO_2 that do occur at HDP are likely below the detection limit of the water vapor analyzers used (Fiorella et al., 2018a). Instead, we suggest that changes in the humidity and moisture history of the HDP airmass are responsible for the strong diurnal cycles in HDP d-excess. For example, cycles in HDP d-excess following PCAP 1 were coincident with cycles in HDP specific humidity. Atmospheric soundings from the Salt Lake City International Airport (Fig. 1) indicate that during this period the top of a second, elevated inversion layer crosses the altitudes of HDP across the diurnal cycle. These periods also correspond to high diurnal spectral power in HDP d-excess, and therefore, we suggest that these variations in the boundary layer structure at HDP are the likely source of diurnal cyclicity observed at HDP.

While the HDP record captures natural hydrologic variability, it is not clear that it provides improved constraints on the d-excess of water vapor in the absence of local emissions, $d_{nat,}$ in the urban environment when CO_2 is elevated during winter. D-excess values remain ~20‰ higher at HDP than observed at UOU for December and January, regardless of atmospheric stability in the Salt Lake Valley. This suggests that HDP and UOU occupy distinct atmospheric layers for much of the winter and are not mixed even when the potential temperature gradient is low. In February, estimated mixing heights suggest that the boundary layer may reach HDP (Fig. 2a); during this period, the d-excess records converge (Fig. 2d). As a result, HDP should not be taken to represent d_{nat} nor background CO_2 concentrations during the winter while these systems are decoupled, but may provide an adequate background of these quantities for the remainder of the year when insolation and mixing heights are higher. Bares et al. (2018) reached a similar conclusion based on a suite of CO_2 and air pollutant measurements. However, while CO_2 concentrations and d-excess values converge between the two sites in

February when mixing heights are high, other variables such as specific humidity, $\delta^{18}O$, and potential temperature, remain distinct (Fig. 2), indicating that these layers may not fully mix throughout the winter season.

The implications of this apparent stratification on determining the CDV fraction of urban humidity depends on the mechanisms driving the divergence between HDP and UOU d-excess values. First, specific humidity was lower at HDP than at UOU. Under a natural condensation process such as adiabatic lifting, d-excess would increase as specific humidity decreases. This effect is non-linear (e.g., Dütsch et al., 2017) and most prominent when specific humidity is low (< 4 g/kg, Fig. 6ab). In this scenario, d-excess at HDP would be greater than at UOU purely due to condensation, and the CDV fraction of urban humidity estimated by Eqn. 3 would be biased high. Our CDV fraction estimates (Table 2), and comparison to a likely range of concentrations based on the plausible range of combustion stoichiometry (Fig. 3), support the conclusion that HDP observations used as a background produce estimates of CDV that are too high. However, the HDP site does capture natural hydrologic variability at high elevation. Due to the decoupling between HDP and UOU observed throughout most of the winter, we suggest that a site at a similar elevation but without nearby anthropogenic emissions may be a more suitable for CDV estimation. Finally, it is not clear how variable CDV amounts would be throughout the urban environment, as fossil fuel emission intensity and fuel sources vary throughout the Salt Lake Valley (Patarasuk et al., 2016). Establishment of additional monitoring sites throughout the urban area would help constrain the spatial variability in CDV amounts.

5. Conclusions

Prior studies indicated that water vapor from fossil fuel combustion may comprise ~10% of urban humidity during winter (Fiorella et al., 2018a; Gorski et al., 2015; Salmon et al., 2017). Stable water vapor isotopes can apportion urban humidity to CDV and "natural" sources, though accurate estimates require knowledge of the amount and isotopic composition of these end members, which is uncertain when measurements are only made in the urban environment. In this study, we tested the hypothesis that a high-elevation site adjacent to Salt Lake City could serve as a background site documenting "natural" d-excess variability in the absence of fossil fuel emissions. We conclude that this hypothesis was incorrect, as it produced estimates of CDV that were too high to be explained by combustion stoichiometry (Fig. 3). However, the two sites showed strong but related contrasts in d-excess variations. A strong inverse correlation between CO_2 and vapor d-excess was observed at UOU (Fig. 2d, 4, 5), which indicates that CDV strongly alters the natural hydrological cycle within the urban system. In contrast, the nearby HDP record shows no signs of being significantly impacted by CDV, and therefore, reflects natural hydrological variability (Fig. 5,6). HDP and UOU d-excess values are distinct when mixing heights are low, indicative of a decoupling between the urban boundary layer and air above the adjacent mountain ranges.

Through these stable isotope measurements, we can fingerprint the impact of water vapor emissions associated with combustion on the urban boundary layer, and directly compare changes of urban boundary layer isotope ratios with changes from natural variability from the HDP site. Though the HDP measurements capture natural variability, however, they may not represent atmospheric processes at an equivalent elevation to UOU. During the winter, the HDP and UOU sites often occupy distinct atmospheric environments as high atmospheric stability isolates the Salt Lake City atmosphere from the layers above. We conclude that measurements at

502 an equal elevation as UOU, but in the absence of emissions, are more likely to improve
503 quantitative estimates of the fraction of urban combustion arising from CDV.
504
505 **Acknowledgments**
506 RPF and GJB received support from NSF grant EF-1241286. IGRA radiosonde data are
507 available from https://www.ncdc.noaa.gov/data-access/weather-balloon/integrated-global-
508 radiosonde-archive. CO_2 observations, RB, and JCL were supported by DOE grant
509 DESC0010624 and NOAA grant NA140AR4310178. UOU and Mt. Baldy meteorological data
510 are available for download from mesowest.utah.edu, CO_2 data are available at air.utah.edu, and
511 vapor isotope data are available at https://osf.io/k47ft. We thank Snowbird Ski and Summer
512 Resort for hosting our HDP measurements. We also thank Dr. David Bowling and Dr. Maria
513 Garcia for providing calibration materials for CO_2 measurements.
514

References

Ackerman, B., 1987. Climatology of Chicago Area Urban-Rural Differences in Humidity. Journal of Climate and Applied Meteorology 26, 427–430. https://doi.org/10.1175/1520-0450(1987)026<0427:COCAUR>2.0.CO;2

Aemisegger, F., Pfahl, S., Sodemann, H., Lehner, I., Seneviratne, S.I., Wernli, H., 2014. Deuterium excess as a proxy for continental moisture recycling and plant transpiration. Atmospheric Chemistry and Physics 14, 4029–4054. https://doi.org/10.5194/acp-14-4029-2014

Aemisegger, F., Spiegel, J.K., Pfahl, S., Sodemann, H., Eugster, W., Wernli, H., 2015. Isotope meteorology of cold front passages: A case study combining observations and modeling. Geophysical Research Letters 42, 5652–5660. https://doi.org/10.1002/2015GL063988

Aemisegger, F., Sturm, P., Graf, P., Sodemann, H., Pfahl, S., Knohl, A., Wernli, H., 2012. Measuring variations of $\delta^{18}O$ and $\delta^{2}H$ in atmospheric water vapour using two commercial laser-based spectrometers: an instrument characterisation study. Atmospheric Measurement Techniques 5, 1491–1511. https://doi.org/10.5194/amt-5-1491-2012

Baasandorj, M., Hoch, S.W., Bares, R., Lin, J.C., Brown, S.S., Millet, D.B., Martin, R., Kelly, K., Zarzana, K.J., Whiteman, C.D., Dube, W.P., Tonnesen, G., Jaramillo, I.C., Sohl, J., 2017. Coupling between Chemical and Meteorological Processes under Persistent Cold-Air Pool Conditions: Evolution of Wintertime $PM_{2.5}$ Pollution Events and N_2O_5 Observations in Utah's Salt Lake Valley. Environmental Science & Technology 51, 5941–5950. https://doi.org/10.1021/acs.est.6b06603

Bailey, A., Chase, T.N., Cassano, J.J., Noone, D., 2011. Changing Temperature Inversion Characteristics in the U.S. Southwest and Relationships to Large-Scale Atmospheric Circulation. Journal of Applied Meteorology and Climatology 50, 1307–1323. https://doi.org/10.1175/2011JAMC2584.1

Bailey, A., Noone, D., Berkelhammer, M., Steen-Larsen, H.C., Sato, P., 2015a. The stability and calibration of water vapor isotope ratio measurements during long-term deployments. Atmospheric Measurement Techniques 8, 4521–4538. https://doi.org/10.5194/amt-8-4521-2015

Bailey, A., Nusbaumer, J., Noone, D., 2015b. Precipitation efficiency derived from isotope ratios in water vapor distinguishes dynamical and microphysical influences on subtropical atmospheric constituents. Journal of Geophysical Research: Atmospheres 120, 9119–9137. https://doi.org/10.1002/2015JD023403

Bares, R., Lin, J.C., Hoch, S.W., Baasandorj, M., Mendoza, D.L., Fasoli, B., Mitchell, L., Catharine, D., Stephens, B.B., 2018. The Wintertime Covariation of CO_2 and Criteria Pollutants in an Urban Valley of the Western United States. Journal of Geophysical Research: Atmospheres 123, 2684–2703. https://doi.org/10.1002/2017JD027917

Barkan, E., Luz, B., 2005. High precision measurements of17O/16O and18O/16O ratios in H2O. Rapid Communications in Mass Spectrometry 19, 3737–3742. https://doi.org/10.1002/rcm.2250

Bengtsson, L., Westerström, G., 1992. Urban snowmelt and runoff in northern Sweden. Hydrological Sciences Journal 37, 263–275. https://doi.org/10.1080/02626669209492586

Bergeron, O., Strachan, I.B., 2012. Wintertime radiation and energy budget along an urbanization gradient in Montreal, Canada. International Journal of Climatology 32, 137–152. https://doi.org/10.1002/joc.2246

Bony, S., Risi, C., Vimeux, F., 2008. Influence of convective processes on the isotopic composition ($\delta^{18}O$ and δD) of precipitation and water vapor in the tropics: 1. Radiative-convective equilibrium and Tropical Ocean–Global Atmosphere–Coupled Ocean-Atmosphere Response Experiment (TOGA-COARE) simulations. Journal of Geophysical Research 113. https://doi.org/10.1029/2008JD009942

Dansgaard, W., 1964. Stable isotopes in precipitation. Tellus 16, 436–468. https://doi.org/10.1111/j.2153-3490.1964.tb00181.x

Dee, D.P., Uppala, S.M., Simmons, A.J., Berrisford, P., Poli, P., Kobayashi, S., Andrae, U., Balmaseda, M.A., Balsamo, G., Bauer, P., Bechtold, P., Beljaars, A.C.M., van de Berg, L., Bidlot, J., Bormann, N., Delsol, C., Dragani, R., Fuentes, M., Geer, A.J., Haimberger, L., Healy, S.B., Hersbach, H., Hólm, E.V., Isaksen, L., Kållberg, P., Köhler, M., Matricardi, M., McNally, A.P., Monge-Sanz, B.M., Morcrette, J.-J., Park, B.-K., Peubey, C., de Rosnay, P., Tavolato, C., Thépaut, J.-N., Vitart, F., 2011. The ERA-Interim reanalysis: configuration and performance of the data assimilation system. Q.J.R. Meteorol. Soc. 137, 553–597. https://doi.org/10.1002/qj.828

Duren, R.M., Miller, C.E., 2012. Measuring the carbon emissions of megacities. Nature Climate Change 2, 560–562. https://doi.org/10.1038/nclimate1629

Dütsch, M., Pfahl, S., Sodemann, H., 2017. The Impact of Nonequilibrium and Equilibrium Fractionation on Two Different Deuterium Excess Definitions. Journal of Geophysical Research: Atmospheres. https://doi.org/10.1002/2017JD027085

Estep, M.F., Hoering, T.C., 1980. Biogeochemistry of the stable hydrogen isotopes. Geochimica et Cosmochimica Acta 44, 1197–1206.

Fiorella, R.P., Bares, R., Lin, J.C., Ehleringer, J.R., Bowen, G.J., 2018a. Detection and variability of combustion-derived vapor in an urban basin. Atmospheric Chemistry and Physics 18, 8529–8547. https://doi.org/10.5194/acp-18-8529-2018

Fiorella, R.P., Poulsen, C.J., Matheny, A.M., 2018b. Seasonal Patterns of Water Cycling in a Deep, Continental Mountain Valley Inferred From Stable Water Vapor Isotopes. Journal of Geophysical Research: Atmospheres. https://doi.org/10.1029/2017JD028093

Fiorella, R.P., Poulsen, C.J., Pillco Zolá, R.S., Jeffery, M.L., Ehlers, T.A., 2015. Modern and long-term evaporation of central Andes surface waters suggests paleo archives underestimate Neogene elevations. Earth and Planetary Science Letters 432, 59–72. https://doi.org/10.1016/j.epsl.2015.09.045

Gorski, G., Strong, C., Good, S.P., Bares, R., Ehleringer, J.R., Bowen, G.J., 2015. Vapor hydrogen and oxygen isotopes reflect water of combustion in the urban atmosphere. Proceedings of the National Academy of Sciences 112, 3247–3252. https://doi.org/10.1073/pnas.1424728112

Graf, P., Wernli, H., Pfahl, S., Sodemann, H., 2019. A new interpretative framework for below-cloud effects on stable water isotopes in vapour and rain. Atmospheric Chemistry and Physics 19, 747–765. https://doi.org/10.5194/acp-19-747-2019

Gralher, B., Herbstritt, B., Weiler, M., Wassenaar, L.I., Stumpp, C., 2016. Correcting Laser-Based Water Stable Isotope Readings Biased by Carrier Gas Changes. Environmental Science & Technology 50, 7074–7081. https://doi.org/10.1021/acs.est.6b01124

Gupta, P., Noone, D., Galewsky, J., Sweeney, C., Vaughn, B.H., 2009. Demonstration of high-precision continuous measurements of water vapor isotopologues in laboratory and remote field deployments using wavelength-scanned cavity ring-down spectroscopy (WS-CRDS) technologyy. Rapid Commun. Mass Spectrom. 9.

606 Hage, K.D., 1975. Urban-Rural Humidity Differences. Journal of Applied Meteorology 14.
607 Hall, S.J., Learned, J., Ruddell, B., Larson, K.L., Cavender-Bares, J., Bettez, N., Groffman,
608 P.M., Grove, J.M., Heffernan, J.B., Hobbie, S.E., Morse, J.L., Neill, C., Nelson, K.C.,
609 O'Neil-Dunne, J.P.M., Ogden, L., Pataki, D.E., Pearse, W.D., Polsky, C., Chowdhury,
610 R.R., Steele, M.K., Trammell, T.L.E., 2016. Convergence of microclimate in residential
611 landscapes across diverse cities in the United States. Landscape Ecology 31, 101–117.
612 https://doi.org/10.1007/s10980-015-0297-y
613 Hendry, M.J., Richman, B., Wassenaar, L.I., 2011. Correcting for Methane Interferences on δ^2H
614 and $\delta^{18}O$ Measurements in Pore Water Using $H_2O_{(liquid)}$–$H_2O_{(vapor)}$ Equilibration Laser
615 Spectroscopy. Analytical Chemistry 83, 5789–5796. https://doi.org/10.1021/ac201341p
616 Horel, J., Splitt, M., Dunn, L., Pechmann, J., White, B., Ciliberti, C., Lazarus, S., Slemmer, J.,
617 Zaff, D., Burks, J., 2002. Mesowest: Cooperative Mesonets in the Western United States.
618 Bulletin of the American Meteorological Society 83, 211–225.
619 https://doi.org/10.1175/1520-0477(2002)083<0211:MCMITW>2.3.CO;2
620 Horita, J., Wesolowski, D.J., 1994. Liquid-vapor fractionation of oxygen and hydrogen isotopes
621 of water from the freezing to the critical temperature. Geochimica et Cosmochimica Acta
622 58, 3425–3437. https://doi.org/10.1016/0016-7037(94)90096-5
623 Johnson, J.E., Rella, C.W., 2017. Effects of variation in background mixing ratios of N_2, O_2, and
624 Ar on the measurement of $\delta^{18}O$–H_2O and δ^2H–H_2O values by cavity ring-down
625 spectroscopy. Atmos. Meas. Tech. 19.
626 Kaiser, H.F., 1958. The varimax criterion for analytic rotation in factor analysis. Psychometrika
627 23, 187–200. https://doi.org/10.1007/BF02289233
628 Keeling, C.D., 1961. The concentration and isotopic abundances of carbon dioxide in rural and
629 marine air. Geochimica et Cosmochimica Acta 24, 277–298.
630 https://doi.org/10.1016/0016-7037(61)90023-0
631 Keeling, C.D., 1958. The concentration and isotopic abundances of atmospheric carbon dioxide
632 in rural areas. Geochimica et Cosmochimica Acta 13, 322–334.
633 https://doi.org/10.1016/0016-7037(58)90033-4
634 Kuttler, W., Weber, S., Schonnefeld, J., Hesselschwerdt, A., 2007. Urban/rural atmospheric
635 water vapour pressure differences and urban moisture excess in Krefeld, Germany.
636 International Journal of Climatology 27, 2005–2015. https://doi.org/10.1002/joc.1558
637 Lauvaux, T., Miles, N.L., Deng, A., Richardson, S.J., Cambaliza, M.O., Davis, K.J., Gaudet, B.,
638 Gurney, K.R., Huang, J., O'Keefe, D., Song, Y., Karion, A., Oda, T., Patarasuk, R.,
639 Razlivanov, I., Sarmiento, D., Shepson, P., Sweeney, C., Turnbull, J., Wu, K., 2016.
640 High-resolution atmospheric inversion of urban CO_2 emissions during the dormant
641 season of the Indianapolis Flux Experiment (INFLUX). Journal of Geophysical Research:
642 Atmospheres 121, 5213–5236. https://doi.org/10.1002/2015JD024473
643 Liu, W., You, H., Dou, J., 2009. Urban-rural humidity and temperature differences in the Beijing
644 area. Theoretical and Applied Climatology 96, 201–207. https://doi.org/10.1007/s00704-
645 008-0024-6
646 Mitchell, L.E., Lin, J.C., Bowling, D.R., Pataki, D.E., Strong, C., Schauer, A.J., Bares, R., Bush,
647 S.E., Stephens, B.B., Mendoza, D., Mallia, D., Holland, L., Gurney, K.R., Ehleringer,
648 J.R., 2018. Long-term urban carbon dioxide observations reveal spatial and temporal
649 dynamics related to urban characteristics and growth. Proceedings of the National
650 Academy of Sciences 115, 2912–2917. https://doi.org/10.1073/pnas.1702393115

Moriwaki, R., Kanda, M., Senoo, H., Hagishima, A., Kinouchi, T., 2008. Anthropogenic water vapor emissions in Tokyo. Water Resources Research 44. https://doi.org/10.1029/2007WR006624

Noone, D., 2012. Pairing Measurements of the Water Vapor Isotope Ratio with Humidity to Deduce Atmospheric Moistening and Dehydration in the Tropical Midtroposphere. Journal of Climate 25, 4476–4494. https://doi.org/10.1175/JCLI-D-11-00582.1

Patarasuk, R., Gurney, K.R., O'Keeffe, D., Song, Y., Huang, J., Rao, P., Buchert, M., Lin, J.C., Mendoza, D., Ehleringer, J.R., 2016. Urban high-resolution fossil fuel CO_2 emissions quantification and exploration of emission drivers for potential policy applications. Urban Ecosystems 19, 1013–1039. https://doi.org/10.1007/s11252-016-0553-1

R Core Team, 2019. R: A language and environment for statistical computing. R Foundation for Statistical Computing, Vienna, Austria.

Rösch, A., Schmidbauer, H., 2016. WaveletComp 1.1: A guided tour through the R package. URL: http://www.hsstat.com/projects/WaveletComp/WaveletComp_guided_tour. pdf.

Salmon, O.E., Shepson, P.B., Ren, X., Marquardt Collow, A.B., Miller, M.A., Carlton, A.G., Cambaliza, M.O.L., Heimburger, A., Morgan, K.L., Fuentes, J.D., Stirm, B.H., Grundman, R., Dickerson, R.R., 2017. Urban emissions of water vapor in winter. Journal of Geophysical Research: Atmospheres 122, 9467–9484. https://doi.org/10.1002/2016JD026074

Schmidt, M., Maseyk, K., Lett, C., Biron, P., Richard, P., Bariac, T., Seibt, U., 2010. Concentration effects on laser-based $\delta^{18}O$ and $\delta^{2}H$ measurements and implications for the calibration of vapour measurements with liquid standards: Concentration effects on CRDS. Rapid Communications in Mass Spectrometry 24, 3553–3561. https://doi.org/10.1002/rcm.4813

Seidel, D.J., Zhang, Y., Beljaars, A., Golaz, J.-C., Jacobson, A.R., Medeiros, B., 2012. Climatology of the planetary boundary layer over the continental United States and Europe. Journal of Geophysical Research: Atmospheres 117, n/a-n/a. https://doi.org/10.1029/2012JD018143

Steen-Larsen, H.C., Sveinbjörnsdottir, A.E., Peters, A.J., Masson-Delmotte, V., Guishard, M.P., Hsiao, G., Jouzel, J., Noone, D., Warren, J.K., White, J.W.C., 2014. Climatic controls on water vapor deuterium excess in the marine boundary layer of the North Atlantic based on 500 days of in situ, continuous measurements. Atmospheric Chemistry and Physics 14, 7741–7756. https://doi.org/10.5194/acp-14-7741-2014

Super, I., Denier van der Gon, H.A.C., Visschedijk, A.J.H., Moerman, M.M., Chen, H., van der Molen, M.K., Peters, W., 2017. Interpreting continuous in-situ observations of carbon dioxide and carbon monoxide in the urban port area of Rotterdam. Atmospheric Pollution Research 8, 174–187. https://doi.org/10.1016/j.apr.2016.08.008

Torrence, C., Compo, G.P., 1998. A Practical Guide to Wavelet Analysis. Bulletin of the American Meteorological Society 79.

Turnbull, J.C., Tans, P.P., Lehman, S.J., Baker, D., Conway, T.J., Chung, Y.S., Gregg, J., Miller, J.B., Southon, J.R., Zhou, L.-X., 2011. Atmospheric observations of carbon monoxide and fossil fuel CO_2 emissions from East Asia. Journal of Geophysical Research: Atmospheres 116, n/a-n/a. https://doi.org/10.1029/2011JD016691

van der Ent, R.J., Savenije, H.H.G., Schaefli, B., Steele-Dunne, S.C., 2010. Origin and fate of atmospheric moisture over continents: Water Resources Research 46. https://doi.org/10.1029/2010WR009127

Venables, W.N., Ripley, B., 2002. Modern applied statistics with S, 4th ed.. ed, Statistics and computing.

Verhulst, K.R., Karion, A., Kim, J., Salameh, P.K., Keeling, R.F., Newman, S., Miller, J., Sloop, C., Pongetti, T., Rao, P., Wong, C., Hopkins, F.M., Yadav, V., Weiss, R.F., Duren, R.M., Miller, C.E., 2017. Carbon dioxide and methane measurements from the Los Angeles Megacity Carbon Project – Part 1: calibration, urban enhancements, and uncertainty estimates. Atmospheric Chemistry and Physics 17, 8313–8341. https://doi.org/10.5194/acp-17-8313-2017

Vogelezang, D.H.P., Holtslag, A.A.M., 1996. Evaluation and model impacts of alternative boundary-layer height formulations. Boundary-Layer Meteorology 81, 245–269. https://doi.org/10.1007/BF02430331

Webster, C.R., Heymsfield, A.J., 2003. Water Isotope Ratios D/H, 18O/16O, 17O/16O in and out of Clouds Map Dehydration Pathways. Science 302, 1742–1745. https://doi.org/10.1126/science.1089496

Whiteman, C.D., Hoch, S.W., Horel, J.D., Charland, A., 2014. Relationship between particulate air pollution and meteorological variables in Utah's Salt Lake Valley. Atmospheric Environment 94, 742–753. https://doi.org/10.1016/j.atmosenv.2014.06.012

Whiticar, M.J., 1999. Carbon and hydrogen isotope systematics of bacterial formation and oxidation of methane. Chemical Geology 161, 291–314. https://doi.org/10.1016/S0009-2541(99)00092-3

Wickham, H., Grolemund, G., 2016. R for data science: import, tidy, transform, visualize, and model data. O'Reilly Media, Inc.

Wolyn, P.G., McKee, T.B., 1989. Deep Stable Layers in the Intermountain Western United States. Monthly Weather Review 117, 461–472. https://doi.org/10.1175/1520-0493(1989)117<0461:DSLITI>2.0.CO;2

Zhao, C.L., Tans, P.P., 2006. Estimating uncertainty of the WMO mole fraction scale for carbon dioxide in air. Journal of Geophysical Research 111. https://doi.org/10.1029/2005JD006003

Tables

Table 1. Summary of water isotope standards used

	$\delta^{18}O$ (‰ VSMOW)	$\delta^{2}H$ (‰ VSMOW)
UOU Standards		
Florida Tap Water	-1.23	-5.51
UT DI2	-15.88	-119.66
HDP Standards		
UT DI	-15.32	-116.03
South Pole Snow	-46.81	-364.31

Table 2. %CDV estimates for urban humidity from UOU and HDP measurements

PCAP ID	d_{nat}, 12 h prior at UOU	d_{nat}, 12 h prior at HDP	d_{obs}, UOU	%CDV($d_{nat,UOU}$)	%CDV($d_{nat,HDP}$)
1	-13.3 ± 6.1‰	19.7 ± 4.5‰	-9.9 ± 4.9‰	-2.1 ± 4.7	14.9 ± 3.6
2a	-8.6 ± 5.2‰	10.7 ± 4.1‰	-17.2 ± 5.3‰	5.0 ± 4.4	14.7 ± 3.8
2b	-7.3 ± 4.6‰	12.4 ± 4.1‰	-23.2 ± 4.4‰	9.3 ± 3.8	18.6 ± 3.5
3	-18.3 ± 6.1‰	20.1 ± 4.5‰	-25.4 ± 6.1‰	4.4 ± 5.3	22.9 ± 4.2
4	0.5 ± 3.8‰	14.9 ± 3.2‰	-2.5 ± 3.9‰	1.7 ± 3.1	9.0 ± 2.8
5	-8.6 ± 5.0‰	14.6 ± 4.0‰	-5.0 ± 4.4‰	-2.1 ± 3.9	10.1 ± 3.2
6	-8.0 ± 5.2‰	12.6 ± 3.8‰	-14.9 ± 5.3‰	4.0 ± 4.3	14.4 ± 3.7
7	0.9 ± 4.2‰	11.7 ± 2.7‰	-9.5 ± 4.3‰	5.8 ± 3.4	11.1 ± 3.0

Figure Captions

Figure 1. Map of the Salt Lake Valley and surrounding mountain ranges. Water isotope and CO_2 measurement locations (UOU and HDP), and the Salt Lake City International Airport data (KSLC) are marked. Winter (DJF) carbon dioxide emission estimates from the HESTIA data product (0.002x0.002° resolution) are provided for Salt Lake County (Patarasuk et al., 2016).

Figure 2. Atmospheric stability, water vapor isotope compositions, CO_2 concentrations, and meteorological variable time series at UOU (black) and HDP (red), presented as six hour moving averages: (a) valley heat deficit (MJ/m^2) and estimated mixing height (m ASL), (b) $\delta^{18}O$ (‰, VSMOW, 1σ uncertainty shaded), (c) d-excess (‰, VSMOW, 1σ uncertainty shaded), (d) CO_2

742 (ppmv), (e) potential temperature (K), (f) specific humidity (g/kg), (g) relative humidity (%), (h)
743 wind speed (m/s) and (i) 500 hPa vertical velocity. Panel (i) was extracted from ERA-Interim
744 Reanalysis data (Dee et al., 2011). PCAP events are shown in grey shading and given an ID (at
745 top) for reference.
746
747 **Figure 3.** Relationship of predicted CDV amounts (ppm) and CO_2 for each PCAP event, using
748 d_{nat} estimates from the 12 hour mean d-excess value from HDP (red) and UOU (black) prior to
749 the initiation of the PCAP. CO_2 concentrations are given as a difference between measured and
750 the DJF minimum value. Dashed lines show 1:1 and 2:1 relationships between CDV and CO_2 in
751 emissions, corresponding to the theoretical range expected from Salt Lake Valley fuels.
752
753 **Figure 4**. D-excess wavelet spectra: (a) UOU wavelet power spectrum of d-excess, (b) HDP
754 wavelet power spectrum of d-excess, (c) UOU cross-wavelet power spectrum of d-excess with
755 CO_2 concentrations. Contour color indicates (cross-)spectral power from low (yellow) to high
756 (blue), with a 95% significance level outlined in white. Arrows in (c) indicate the phase
757 relationship between CO_2 and d-excess, with arrows pointing right (left) indicating that the time
758 series are in phase (out of phase).
759
760 **Figure 5.** Biplots of principal components (PCs) 1-3 and the relationship between isotopic
761 composition and q for UOU (top half, a-b) and HDP (bottom half, c-d). For both sites, PCs 1-3
762 (a,b for UOU; c,d for HDP) show the correlation structure between d-excess, $\delta^{18}O$, q, relative
763 humidity (RH), CO_2 concentration, and the ERA-Interim 500 hPa vertical velocity. Highly
764 correlated variables point in the same direction, anti-correlated variables point in opposite

765 directions, and uncorrelated variables are orthogonal. The length of each arrow corresponds to
766 the relative importance of those variables to each principal component. Data corresponding to
767 PCAP (non-PCAP) periods are plotted as turquoise circles (orange triangles). PCAP periods
768 diverge from non-PCAP periods along the CO_2 axis for UOU and the 500 hPa vertical velocity
769 axis for HDP.
770
771 **Figure 6.** Isotope distributions between UOU and HDP. The top row shows the relationship
772 between d-excess and specific humidity (q, mmol/mol) for UOU (a) and HDP (b), while the
773 bottom row shows the joint isotope distributions of d-excess against $\delta^{18}O$ for UOU (c) and HDP
774 (d). In all panels, data points are colored by the concurrent CO_2 concentrations at that site.
775 Models of the isotope ratio under Rayleigh distillation conditions (solid line) and mixing
776 between tropical and dry continental end members (dashed) are provided for all panels, while
777 panels (a) and (b) also include modeled compositions with the addition of CDV (dotted).

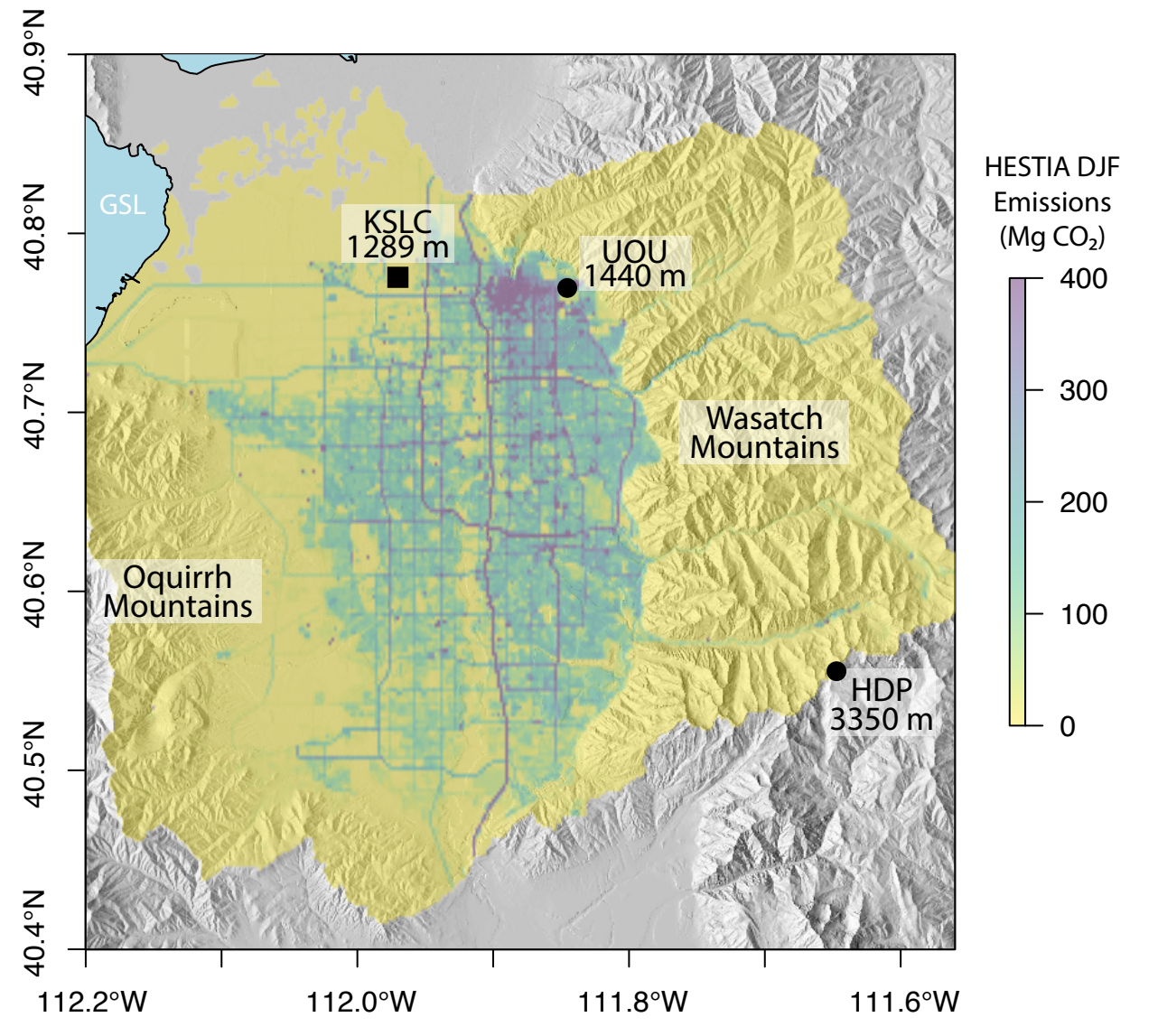
GSL
KSLC
1289 m
UOU
1440 m
Wasatch
Mountains
Oquirrh
Mountains
HDP
3350 m
HESTIA DJF
Emissions
(Mg CO2)
400
300
200
100
0
40.9°N
40.8°N
40.7°N
40.6°N
40.5°N
40.4°N
112.2°W
112.0°W
111.8°W
111.6°W

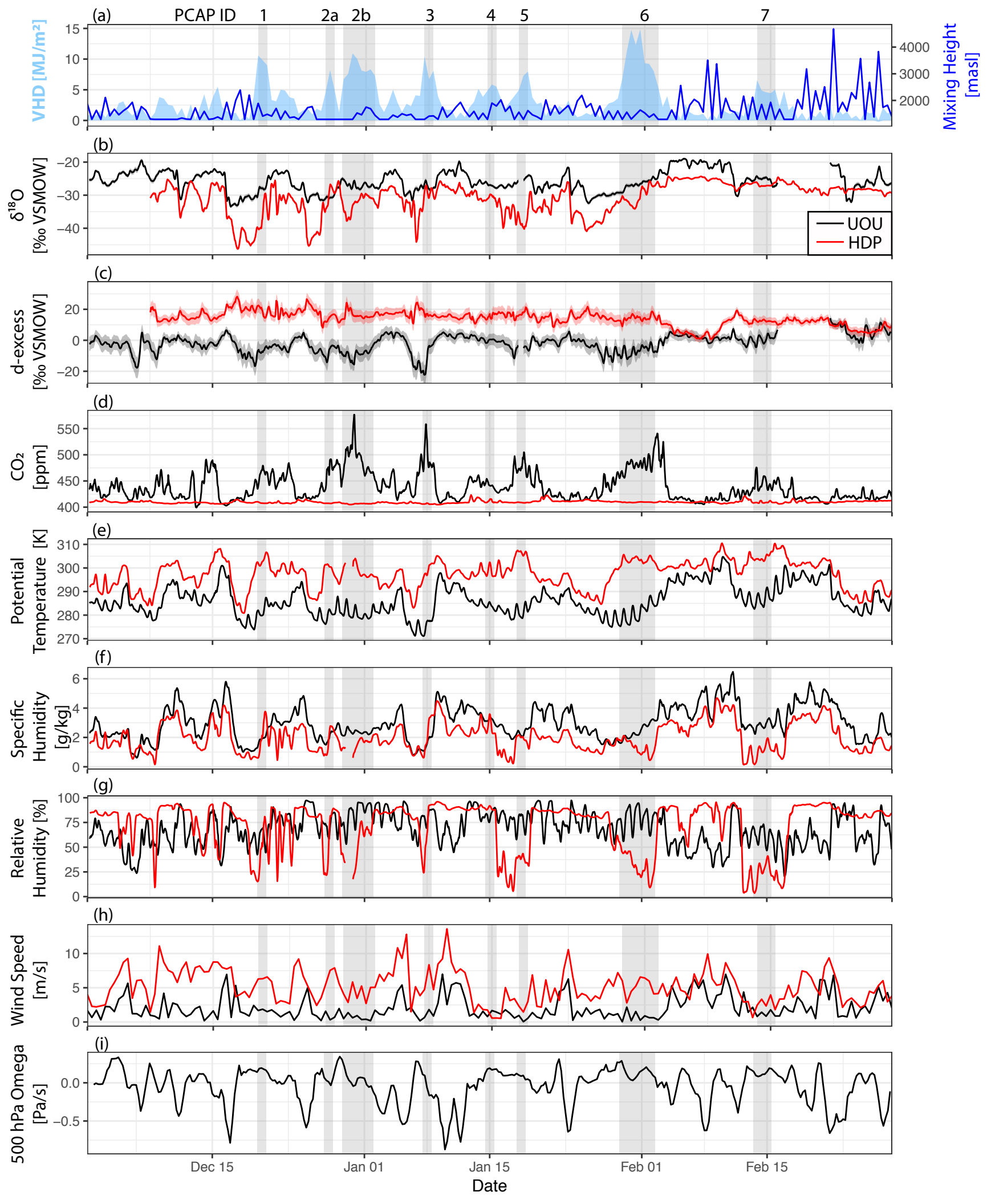
(a)
PCAP ID
1
2a
2b
3
4
5
6
7
VHD [MJ/m²]
Mixing Height [masl]
(b)
δ18O [‰ VSMOW]
UOU
HDP
(c)
d-excess [‰ VSMOW]
(d)
CO2 [ppm]
(e)
Potential Temperature [K]
(f)
Specific Humidity [g/kg]
(g)
Relative Humidity [%]
(h)
Wind Speed [m/s]
(i)
500 hPa Omega [Pa/s]
Dec 15
Jan 01
Jan 15
Feb 01
Feb 15
Date

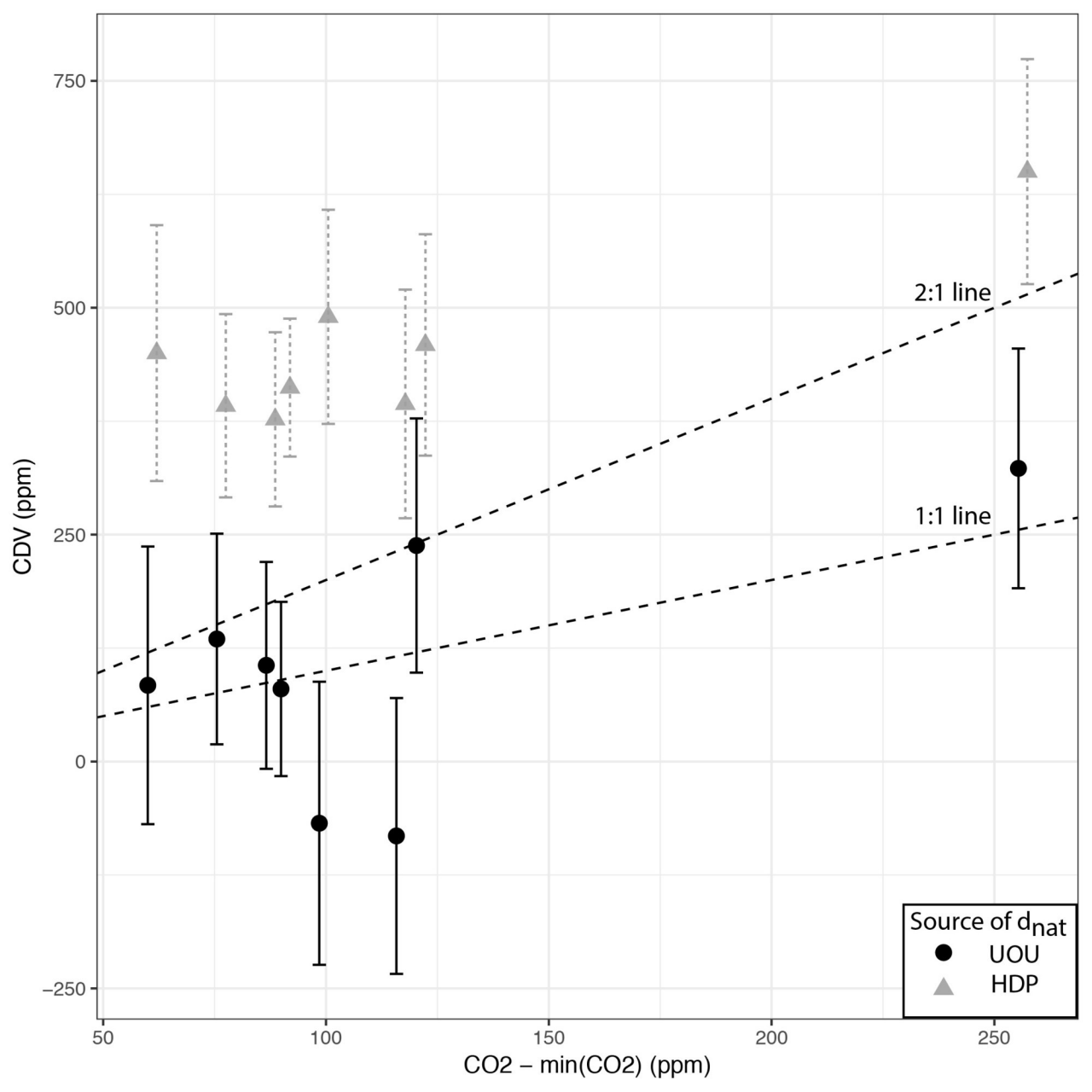
750
500
250
0
−250
CDV (ppm)
50
100
150
200
250
CO2 − min(CO2) (ppm)
2:1 line
1:1 line
Source of d_{nat}
UOU
HDP

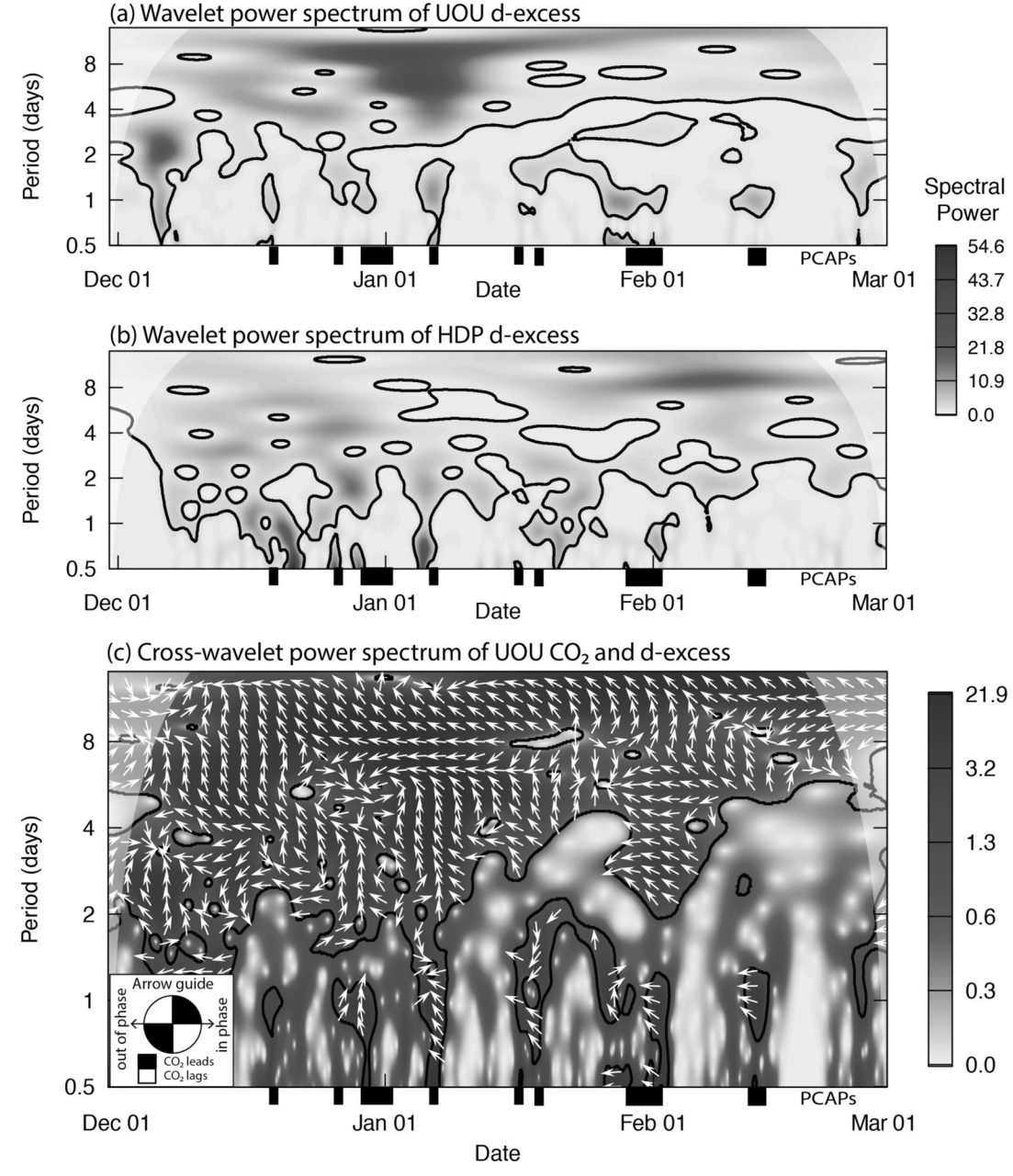
(a) Wavelet power spectrum of UOU d-excess
Period (days)
8
4
2
1
0.5
Spectral Power
54.6
43.7
32.8
21.8
10.9
0.0
PCAPs
Dec 01
Jan 01
Feb 01
Mar 01
Date
(b) Wavelet power spectrum of HDP d-excess
Period (days)
8
4
2
1
0.5
PCAPs
Dec 01
Jan 01
Feb 01
Mar 01
Date
(c) Cross-wavelet power spectrum of UOU CO_2 and d-excess
Period (days)
8
4
2
1
0.5
21.9
3.2
1.3
0.6
0.3
0.0
Arrow guide
out of phase
in phase
CO_2 leads
CO_2 lags
PCAPs
Dec 01
Jan 01
Feb 01
Mar 01
Date

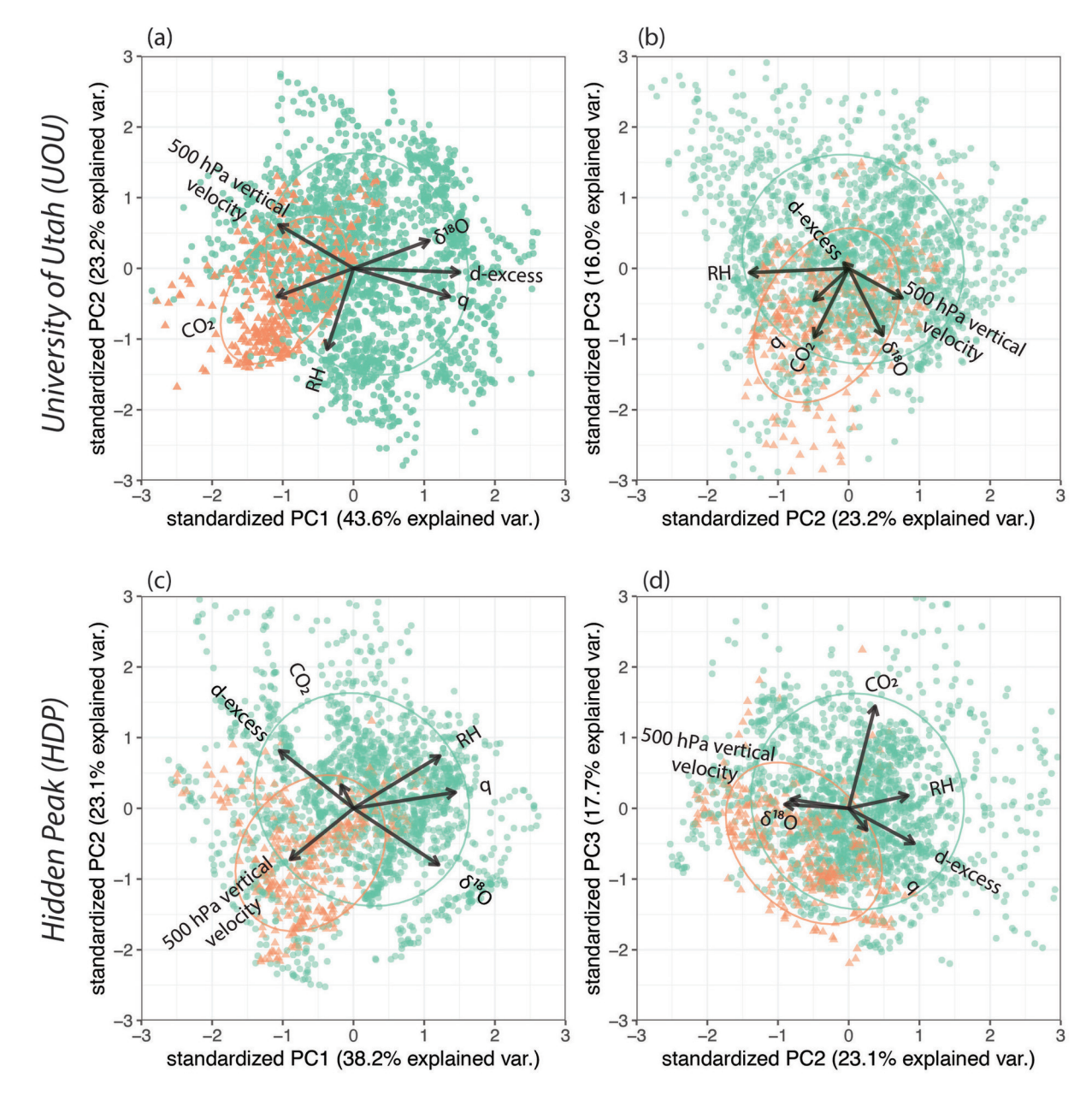
University of Utah (UOU)
Hidden Peak (HDP)
(a)
(b)
(c)
(d)
standardized PC2 (23.2% explained var.)
standardized PC1 (43.6% explained var.)
standardized PC3 (16.0% explained var.)
standardized PC2 (23.2% explained var.)
standardized PC2 (23.1% explained var.)
standardized PC1 (38.2% explained var.)
standardized PC3 (17.7% explained var.)
standardized PC2 (23.1% explained var.)
500 hPa vertical velocity
δ18O
d-excess
q
CO2
RH

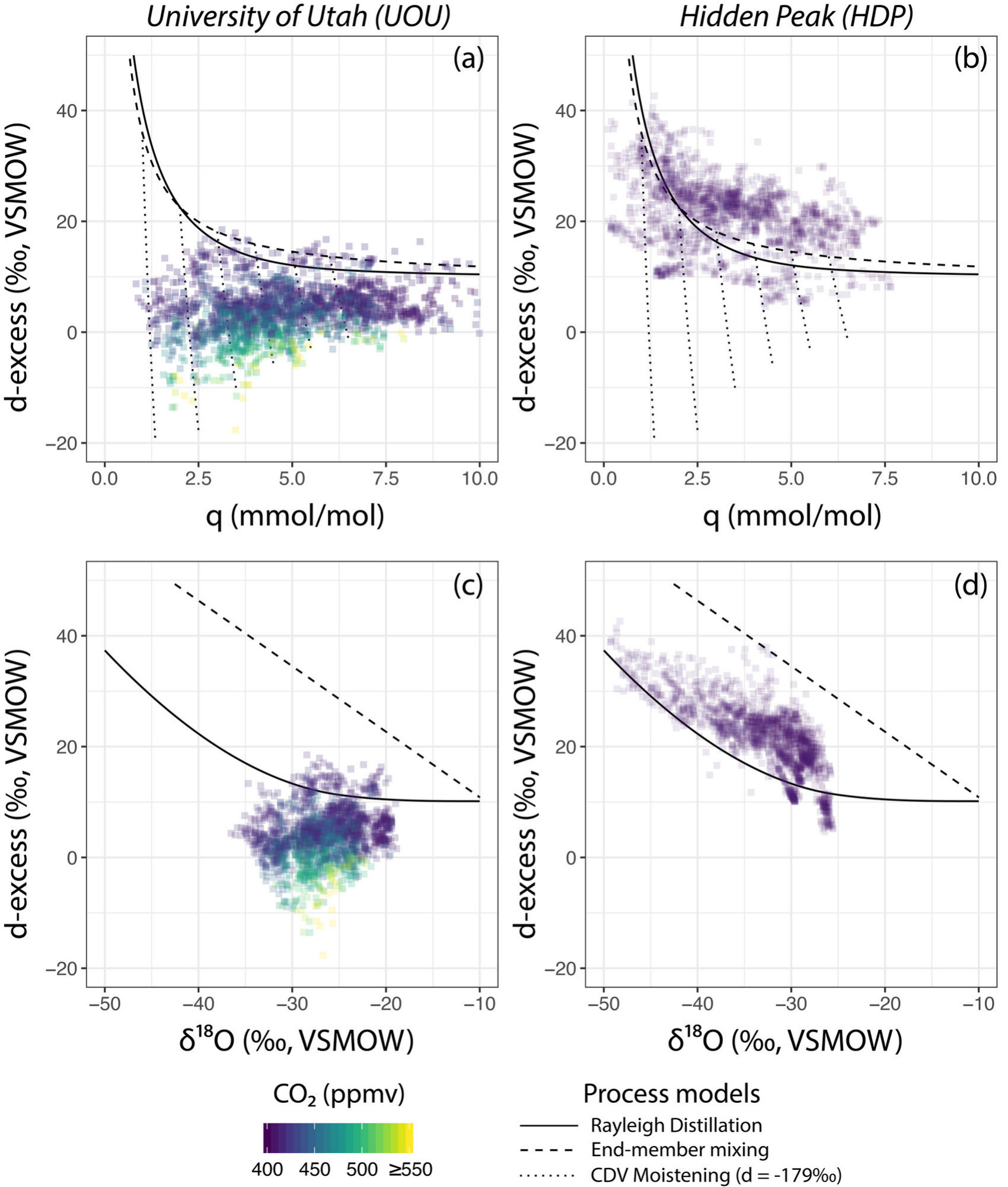
University of Utah (UOU)
Hidden Peak (HDP)
(a)
(b)
(c)
(d)
d-excess (‰, VSMOW)
q (mmol/mol)
δ18O (‰, VSMOW)
40
20
0
−20
0.0
2.5
5.0
7.5
10.0
−50
−40
−30
−20
−10
CO2 (ppmv)
400 450 500 ≥550
Process models
Rayleigh Distillation
End-member mixing
CDV Moistening (d = -179‰)